Fluorinated Fullerenes: Sources of Donor−Acceptor Dyads with [18]Trannulene Acceptors for Energy- and Electron-Transfer Reactions

Dirk M. Guldi,*,† Massimo Marcaccio,‡ Francesco Paolucci,*,‡ Demis Paolucci,‡ Jeff Ramey,|| Roger Taylor,*,§ and Glenn A. Burley§

Institute for Physical and Theoretical Chemistry, Universität Erlangen, 91058 Erlangen, Germany, Dipartimento di Chimica "G. Ciamician", Università di Bologna and INSTM, Via Selmi 2, 40126 Bologna, Italy, Radiation Laboratory, University of Notre Dame, Notre Dame, Indiana 46556, and Chemistry Department, University of Sussex, Brighton BN1 9QJ, U.K.

Received: June 20, 2005; In Final Form: August 23, 2005

Fine-tuned control over the donor strength in a series of trannulenes-based donor−acceptor ensembles is used to alter the deactivation path of the photoexcited-state chromophore and to modulate the rates of intramolecular electron transfer. For the first time, a detailed analysis of emission spectra, time-dependent spectroscopic measurements, and electrochemistry prove spectroscopically and kinetically that trannulenes can serve, in a manner similar to C_{60} and C_{60} monoadducts, as both electron and also as energy acceptor in donor−acceptor ensembles, producing widely different electron-transfer regimes. This investigation also shows that the integration of trannulenes, as a versatile electron-acceptor building block, consistently produces charge recombination in the inverted Marcus region.

Introduction

The design and construction of nanoscale molecular devices that transduce light energy into useful chemical work with high efficiency is a major goal of the physical and chemical sciences. Photosynthesis achieves this goal by a complex series of energy-absorbing and electron-transfer events resulting in the production of cellular fuel in the form of adenosine triphosphate. There is now widespread interest in mimicking the basic processes of photosynthesis by linking moieties that can, upon photoexcitation, transfer and store energy/electrons.[1,2]

With the advent of fullerenes a new energy/electron-accepting functionality became readily available. This three-dimensional carbon allotrope exhibits many characteristics[1−3] amenable for the construction of artificial photovoltaic devices such as the following: significant absorptions in the UV region—with extinction coefficients exceeding 50.000 $M^{-1}cm^{-1}$; spin-forbidden transitions in the visible region typically characterized by low oscillator strength (i.e., <1000 $M^{-1}cm^{-1}$).[4]

These physical properties have been exploited in solar conversion systems when integrated with chromophoric components, via covalent attachment of suitable addends.[5] However, saturation of one or more of the fullerene carbon−carbon double bonds as a consequence of derivatization usually results in a reduction in electron affinity of the carbon cage—approximately 0.1 V per functionalizing addend.[6] If, however, a large number of strongly electron-withdrawing addends are attached to the cage, then the effect of hybridization change can be outweighed. This has in particular been achieved through the fluorination of fullerenes, where the small size of the electronegative addends allows substantial polyaddition to take place. As a consequence the reduction potentials of C_{60}, $C_{60}F_{18}$, $C_{60}F_{36}$, and $C_{60}F_{48}$ are anodically shifted (−0.59, 0.33, 0.10, and 0.78 V, respectively; reduction potentials measured in dichloromethane, vs SCE).[7]

The recent discovery of the family of trannulenes comprising an 18π annulene in the all-trans configuration (Chart 1) provided a new opportunity for the design of organic-based photovoltaic devices.[3,8] Trannulenes have high electron affinities, enabling them to stabilize charged entities more effectively than conventional fullerene derivatives. Additionally trannulenes have rich visible absorptions attributed to the diatropic 18π annulene substructure.[3,8,9] Coupled with a mild preparative methodology producing radial three-dimensional architectures, these molecules could be a useful molecular building block for tailor-made components for optoelectronics, molecular-scale logic gates, and sensor design. Preliminary electron-transfer investigations of an extended tetrathiafulvalene trannulene dyad confirmed the ability of these remarkable molecules to accept a charged entity and store the photoexcitation energy in a long-lived charge-separated state.[8a]

We now describe the electrochemical and photophysical characterization of a novel family of multicomponent donor−acceptor trannulenes, incorporating a range of electro- and photoactive functionalities (Chart 2), whose preparation was recently described.[8c] In particular, the chosen electron donors are characterized by different donor ability that range from pyrene (+1.41 V) to perylene (+0.89 V) and finally to ferrocene (+0.44 V). We will demonstrate that, depending on the relative energies of the lowest excited state or of the charge-separated state, we can fine-tune the outcome of the deactivation of the excited-state chromophore, that is, an all-energy versus electron transfer.

Results and Discussion

Synthesis. Formation of the trannulenes (Chart 1) was as follows: ethyl aryl malonates, formed by initial reaction of the

* To whom correspondence should be addressed. E-mail: dirk.guldi@chemie.uni-erlangen.de (D.M.G.); Francesco.Paolucci@unibo.it (F.P.); R.Taylor@sussex.ac.uk (R.T.).

† Universität Erlangen.

‡ Università di Bologna and INSTM.

|| University of Notre Dame.

10.1021/jp053295h CCC: $30.25
Published on Web 10/08/2005

CHART 1: Schlegel Diagram of [18]Trannulenes (R = CO_2Et, X = CO_2R^1, R^1 = Electron Donor Group, ● = F)

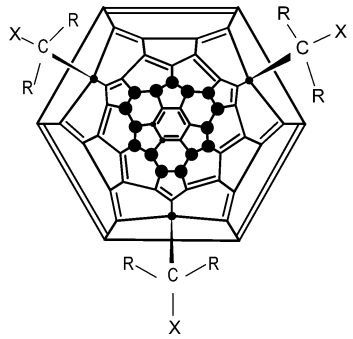

CHART 2: Electron-Donor Substituents (R^1) of the Trannulene. (a) Reference, *m*-Dimethoxybenzene; (b) Pyrene; (c) Ferrocene; (d) Perylene

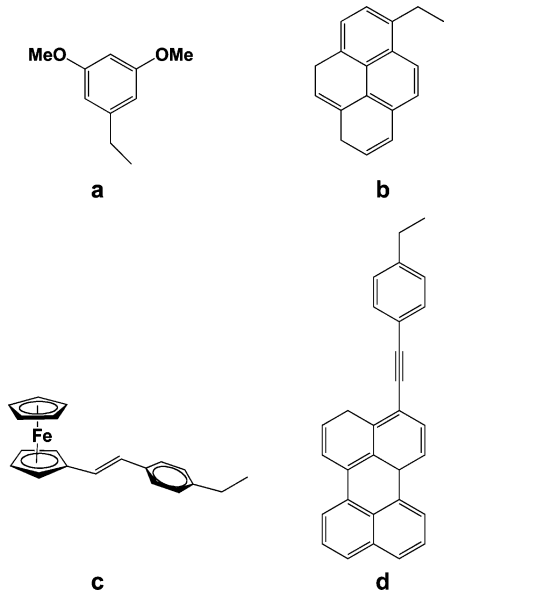

SCHEME 1: Reaction Sequence for the Formation of the Trannulene Dyads

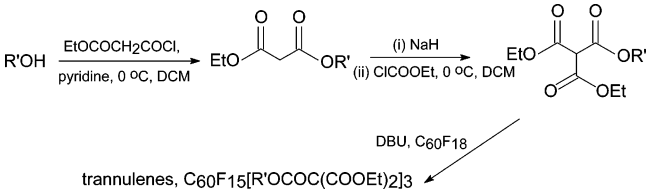

hydroxymethyl aromatics RCH_2OH (see Chart 2 for RCH_2O- groups) with ethyl chloromalonyl chloride, were reacted with ethyl chloroformate to give tertiary methanetricarboxylate esters. These were reacted with $C_{60}F_{18}$ in the presence of DBU to produce the desired trannulenes $C_{60}F_{15}Y_3$ (Scheme 1).[8] In the following discussion, the description of the trannulenes is simplified, so that $C_{60}F_{15}-$pyrene, etc., refers to the *trannulene* in which the R group is pyreneCH_2-.

Electrochemistry. The electrochemical properties of $C_{60}F_{15}-$pyrene, $C_{60}F_{15}-$perylene, and $C_{60}F_{15}-$ferrocene dyads, together with reference compound $C_{60}F_{15}-$*m*-dimethoxybenzene, were investigated by cyclic voltammetry (CV) and spectroelectrochemical experiments. Suitable experimental conditions, which include ultradry solvents, electrolytes with very high oxidation resistance and low nucleophilicity, were used so as to stabilize the electrochemically generated radical cations and anions of the above trannulenes.[13] Under similar conditions, we recently

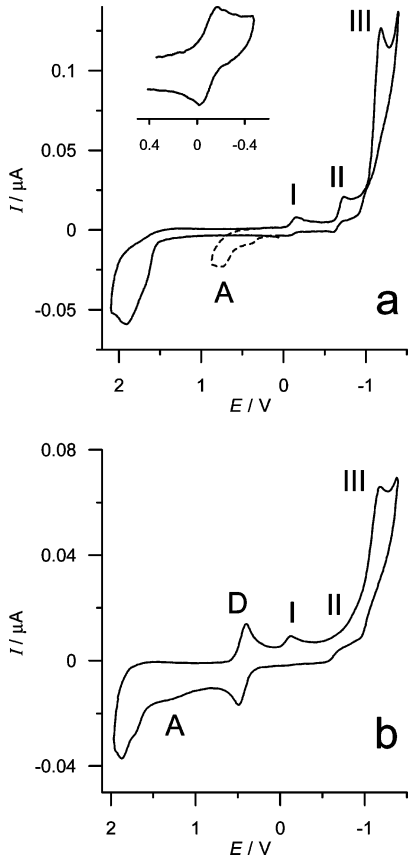

Figure 1. Cyclic voltammetric curves of (a) 0.5 mM $C_{60}F_{15}-$*m*-dimethoxybenzene and (b) 0.5 mM $C_{60}F_{15}-$ferrocene, 0.1 (TBA)PF_6/DCM solutions. Working electrode: platinum disk (diameter, 0.125 mm). T = 298 K. Scan rate = 1 V s^{-1}.

succeeded in observing the reversible generation of the di- and trications of C_{60}.[10] The results of the CV investigations are displayed in Figures 1 and 2, and the relevant redox potential data are collected in Table 1.

Figure 1a shows the CV curve of $C_{60}F_{15}-$*m*-dimethoxybenzene, which is used as a model for the electrochemical behavior of the trannulenic unit in the dyads. Three irreversible reduction peaks are observed—all denoted by Roman numbers. When the potential scan is limited so as to include only the first peak (i.e., see inset in Figure 1a), the latter is reversible and corresponds to a one-electron process, with $E_{1/2} = -0.09$ V. By contrast, in the wide-scan CV curves, all reductions are irreversible up to scan rates as high as 100 V s^{-1}. Peaks II and III, with $E_p = -0.72$ and -1.18 V, are associated with two-electron and multielectron charge-transfer processes, respectively. Such peaks shift to more negative potentials by approximately 30 mV for a 10-fold increase of scan rate (up to 100 V s^{-1}), thus suggesting the occurrence of fast follow-up chemical reactions coupled to the primary reduction processes, according to the so-called EC mechanism.[11] The anodic peak A is only observed in the reverse scan when the forward scan includes peak III and was therefore attributed to an electroactive species emerging from the above chemical degradation of multielectron-reduced trannulenes. Such a reaction is most likely attributed to heterolytic C−F bond cleavage and subsequent loss of fluoride ions, as previously proposed in the case of $C_{60}F_{48}$[7a] and of other classes of perfluorinated fullerenes such as $C_{60}F_{18}$, $C_{60}F_{18}O$, and $C_{60}F_{36}$.[7d] In contrast, the multielectron irreversible peak observed in the positive potential region (E_p = 1.91 V) was assigned to the pristine trannulenic moiety in line with the

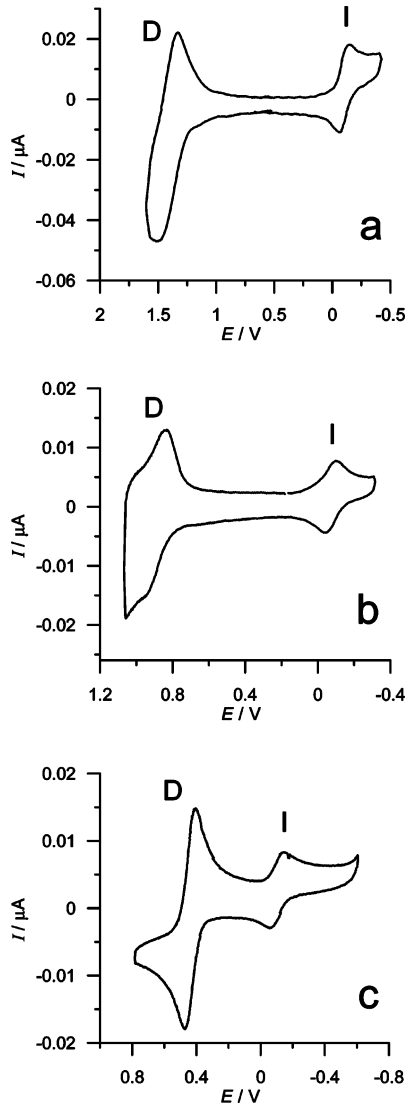

Figure 2. Cyclic voltammetric curves of (a) 0.5 mM $C_{60}F_{15}$−pyrene, (b) 0.5 mM $C_{60}F_{15}$−perylene, and (c) 0.5 mM $C_{60}F_{15}$−ferrocene, in either 0.1 M (TBA)AsF_6/DCM or 0.1 M (TBA)PF_6/TCE solutions. Working electrode: platinum disk (diameter, 0.125 mm). $T = 298$ K. Scan rate = 1 V s^{-1}.

TABLE 1: Electrochemical Potentials (vs SCE)

	$E_{1/2}$/V			
	I	II[c]	III[c]	D[d]
reference[a]	−0.09	−0.72	−1.18	
$C_{60}F_{15}$−pyrene[b]	−0.10	−0.75	−1.14	1.41
$C_{60}F_{15}$−perylene[b]	−0.08	−0.72	−1.16	0.89
$C_{60}F_{15}$−ferrocene[a]	−0.10	−0.72sh	−1.81	0.44

[a] Data collected in 0.05 M (TBA)PF_6/TCE, at 1 V s^{-1}, at 298 K. [b] Data collected in 0.05 M (TBA)AsF_6/DCM, at 1 V s^{-1}, at 298 K. [c] E_p for quasi-reversible or totally irreversible peaks. [d] Three-electron process.

voltammetric behavior of other trannulene derivatives carrying nonelectroactive substituents.[8]

All dyads display analogously a similar highly irreversible CV pattern, characterized by three reduction peaks in the region of negative potentials and an oxidation peak in the positive potentials one, as exemplified by the CV curve of $C_{60}F_{15}$−ferrocene shown in Figure 1b. Peak II is in this case only observed as a shoulder of the much more intense peak III. All processes are located at potentials similar to that in the reference compound—see Table 1—and were accordingly attributed to the

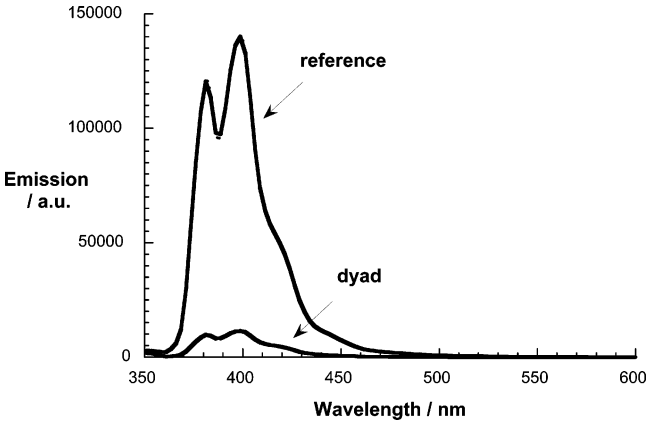

Figure 3. Room-temperature steady-state fluorescence spectra of the pyrene reference and the $C_{60}F_{15}$−pyrene dyad in aerated DCM with matching absorption at the 337 nm excitation wavelength (i.e., $OD_{337nm} = 0.2$).

trannulenic moiety. Not unexpectedly, however, the CV curves of all dyads also display an additional reversible oxidation peak (peak D in Figures 1b and 2) that is located at less positive potentials than the oxidation peak attributed to the trannulene moiety. Such a process corresponds in all dyads to a three-electron oxidation peak, as estimated by comparison with peak I, and was therefore ascribed to the oxidation of the donor units. The CV curves of pyrene−, perylene−, and ferrocene−$C_{60}F_{15}$ dyads are shown in Figure 2a−c, where the potential scan was limited in order to include both the reversible donor-centered oxidation peak D and the reversible trannulene-centered reduction peak I. Interestingly, the three one-electron oxidation processes that are comprised within peak D occur at very close potentials, thus indicating the absence of sizable mutual interactions between the units in the ground state.

Photochemistry. While pyrene ($\Phi = 0.4$) and perylene ($\Phi = 0.4$) exhibit distinct and strong fluorescence, which we employed consequently as sensitive markers for the intramolecular transfer reactions, the lack of ferrocene-centered fluorescence necessitated the use of the rather weak fluorescing features of $C_{60}F_{15}$−*m*-dimethoxybenzene ($\Phi = 1.1 \times 10^{-4}$). Representative examples in air-equilibrated dichloromethane are summarized in Figures 3 and S1 (Supporting Information). We noted that for pyrene and perylene the fluorescence quenching in the corresponding $C_{60}F_{15}$−donor dyads is close to quantitative, that is, ranging between 92 and 98%. Important is the fact that, despite the strong fluorescence quenching, all emission features are preserved and exhibited very little perturbation in comparison to the precursor materials that we used as reference systems. On the other hand, in the $C_{60}F_{15}$−ferrocene dyad the quenching is only around 50%. The limited stability of the $C_{60}F_{15}$ derivatives in protic and/or polar media prevented us from testing a broader spectrum of solvents.

Time-resolved fluorescence measurements complemented the fluorescence assays. In these experiments we compared the decay of the characteristic features of the photoexcited chromophore in the reference systems with those in the $C_{60}F_{15}$−donor dyads. For example, in air-equilibrated dichloromethane the pyrene and perylene references exhibit fluorescence lifetimes of 34 ± 1 and 2.1 ± 0.1 ns, respectively. These values are well in line with those reported in the literature.[12] In the corresponding dyads the fluorescence−time profiles are best fitted (i.e., with χ^2 values of at least 1) by a monoexponential rate law. The lifetimes are, however, reduced to 0.2 ± 0.05 ns ($C_{60}F_{15}$−pyrene) and 0.1 ± 0.05 ns ($C_{60}F_{15}$−perylene). Figure 4 compares the fluorescence−time profiles for pyrene and $C_{60}F_{15}$−pyrene.

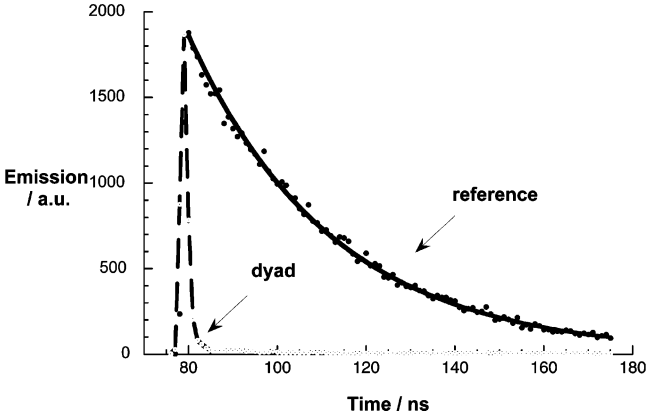

Figure 4. Time-resolved fluorescence decay of the pyrene reference and the $C_{60}F_{15}$−pyrene dyad in aerated DCM following 337 nm laser excitation of the pyrene moiety.

The overall observation further confirms the steady-state quenching. Similarly, the $C_{60}F_{15}$-centered lifetime is 0.46 ± 0.05 ns, relative to 1.6 ± 0.1 ns seen in the $C_{60}F_{15}$−*m*-dimethoxybenzene reference.

To conclude, the newly synthesized series of $C_{60}F_{15}$−donor ensembles display efficient and rapid intramolecular deactivation of their photoexcited chromophores in the steady-state and time-resolved fluorescence experiments with quantum efficiencies (Φ) of 99.4% ($C_{60}F_{15}$−perylene), 95.3% ($C_{60}F_{15}$−pyrene), and 71.5% ($C_{60}F_{15}$−ferrocene). This trend is similar to our recent report regarding intramolecular electron-transfer events within a $C_{60}F_{15}$−extTTF ensemble.[8a] Drawing assumptions—whether electron transfer or competitively energy transfer governs the fate of the photoexcited dyads—that are based only on the fluorescing features is, nevertheless, unfeasible, especially taking into account the different donor ability of the tested electron donors. Thus to shed light onto the product of fluorescence quenching, we investigated the $C_{60}F_{15}$−donor dyads by means of transient absorption measurements (i.e., throughout the pico- to microsecond time range).

First we tested the $C_{60}F_{15}$−*m*-dimethoxybenzene reference in transient absorption measurements following short 532 nm laser pulses (i.e., 532 nm). Figure 5 shows the different transient absorptions after several time delays. Obviously, immediately after the laser pulse we observe bleaching in the 600−700 nm range, which corresponds to the ground-state features of the $C_{60}F_{15}$ moiety. This bleaching is flanked by new transitions in the blue (i.e., 540 nm) and red (i.e., 745 nm) that diminishes with time. We assign these features to the singlet excited transitions of $C_{60}F_{15}$−*m*-dimethoxybenzene. In line with fluorescence experiments the singlet excited state is metastable and decays monoexponentially to yield the triplet manifold. From the analysis at different wavelengths throughout the 550−800 nm region we determine a relatively short lifetime of 0.95 ± 0.1 ns. At first glance spectral transformation between the two manifolds is dominated only by fading features. A closer inspection of the red region, for example, discloses, however, that the 745 nm peak red shifts to about 760 nm. We assign the features at the end of the picosecond time scale (i.e., 4000 ps) to the $C_{60}F_{15}$−*m*-dimethoxybenzene triplet—analogous to data published for C_{60} and most of its derivatives.[4]

Independent confirmation for the triplet assignment evolved from parallel nanosecond transient spectroscopy (i.e., 8 ns laser pulses at 532 nm). The differential absorption spectrum shown in Figure S2 (Supporting Information) and especially the peak location at 770 nm is in excellent agreement with the spectrum

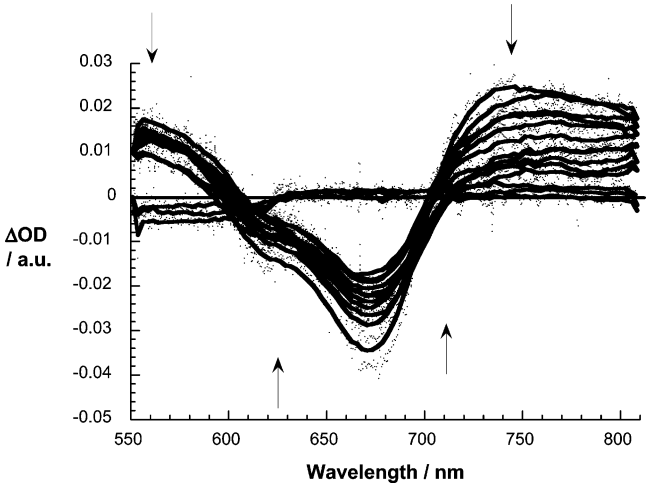

Figure 5. Differential absorption spectrum (visible) obtained upon picosecond flash photolysis (532 nm) of $\sim 1.0 \times 10^{-5}$ M solutions of the $C_{60}F_{15}$−*m*-dimethoxybenzene reference in nitrogen-saturated DCM with several time delays between 50 and 4000 ps at room temperature. The spectrum corresponds to the changes that are associated with the transformation of the $C_{60}F_{15}$−*m*-dimethoxybenzene singlet excited state to the corresponding triplet excited state.

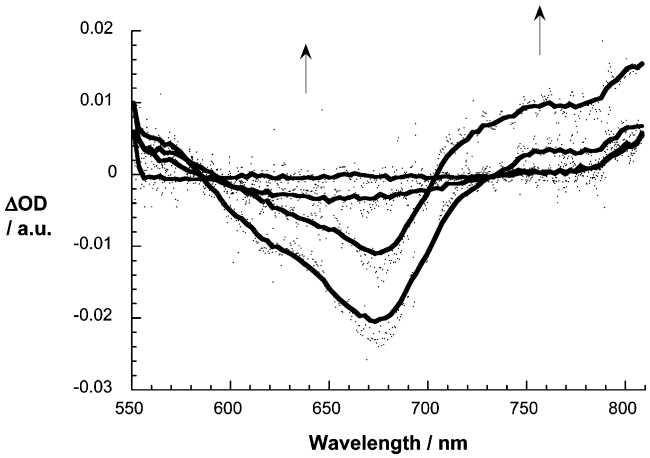

Figure 6. Differential absorption spectrum (visible) obtained upon picosecond flash photolysis (532 nm) of $\sim 1.0 \times 10^{-5}$ M solutions of $C_{60}F_{15}$−ferrocene dyad in nitrogen-saturated DCM with several time delays between 50 and 500 ps at room temperature. The spectrum corresponds to the changes that are associated with the transformation of the $C_{60}F_{15}$−*m*-dimethoxybenzene singlet excited state to the radical ion-pair state.

at the end of the picosecond time scale. In the absence of oxygen we measured a triplet lifetime of 19 ± 1 μs.

Figure 6 demonstrates that the differential absorption changes following 532 nm photoexcitation of $C_{60}F_{15}$−ferrocene are distinctly different from that summarized for the $C_{60}F_{15}$−*m*-dimethoxybenzene reference. Initially, we still see the singlet−singlet features of the fullerene core. However, instead of seeing the slow intersystem crossing dynamics, which convert the singlet to the triplet manifold, we see an accelerated decay (i.e., 0.46 ± 0.05 ns) that also reveals characteristics, which are different from the triplet spectrum seen for $C_{60}F_{15}$−*m*-dimethoxybenzene. We ascribe these new features, on the basis of spectroelectrochemical investigations, to the radical ion pair. The differential absorption spectrum of $C_{60}F_{15}$−*m*-dimethoxybenzene after exhaustive bulk electrolysis at $E = -0.2$ V, corresponding to the one-electron reduction of the trannulenic unit (Figure 7), shows in fact the same features. Notice that the corresponding spectrum of ferrocenium radical cation is mainly characterized by a strong positive change in

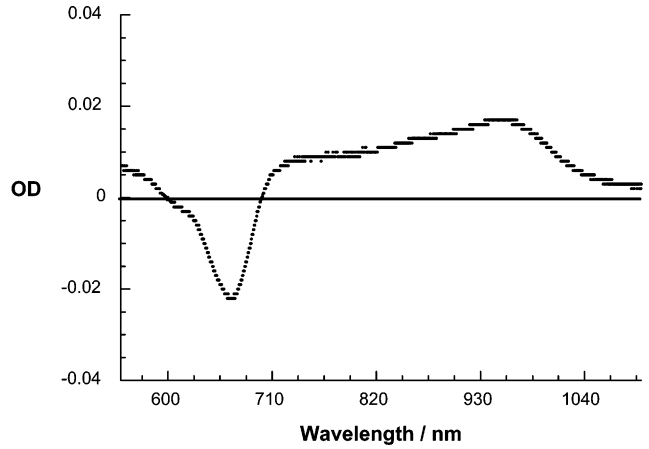

Figure 7. Differential electronic absorption spectrum of a 0.5 mM $C_{60}F_{15}$−*m*-dimethoxybenzene, 0.1 M (TBA)PF_6/DCM solutions after exhaustive bulk electrolysis at $E = -0.2$ V (corresponding to the one-electron reduction of the trannulenic unit), recorded at 298 K.

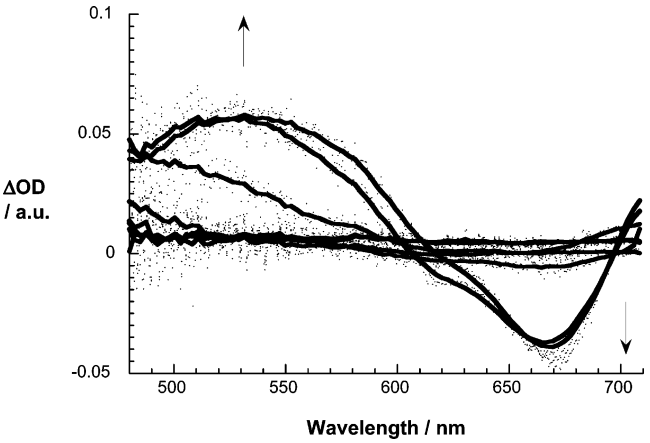

Figure 8. Differential absorption spectrum (visible) obtained upon picosecond flash photolysis (355 nm) of $C_{60}F_{15}$−pyrene dyad ($\sim 1.0 \times 10^{-5}$ M) in nitrogen-saturated DCM with several time delays between 50 and 200 ps at room temperature. The spectrum corresponds to the changes that are associated with the transformation of the pyrene singlet excited state to the $C_{60}F_{15}$−*m*-dimethoxybenzene singlet excited state.

the UV region (Figure S3, Supporting Information) and, consequently, contributes only marginally to the transient absorption spectra shown in Figure 6.

The radical ion pair features are metastable and decay with lifetimes > 6 ns (>1.6×10^8 s^{-1}) back to the singlet ground state. Complementary nanosecond experiments—with a time resolution of ~25 ns—failed to show any stable radical ion pair signatures.

For $C_{60}F_{15}$−pyrene and $C_{60}F_{15}$−perylene the situation is quite different. Most importantly, choosing 337 nm laser excitation—instead of 532 nm—results in the predominant excitation of the pyrene and perylene moieties, respectively. Consequently, we notice at early times in the differential absorption changes, following picosecond excitation of $C_{60}F_{15}$−pyrene and $C_{60}F_{15}$−perylene—see Figures 8 and 9—the singlet−singlet features of both chromophores. In the case of perylene the following appreciable singlet characteristics evolve: bleaching < 490 nm and a new maximum ~ 505 nm. For pyrene, on the other hand, the singlet−singlet maximum is seen at 480 nm, while the ground-state bleaching falls in a region that is outside of the accessible apparatus region (i.e., <450 nm). Relative to the reference compounds, both singlet fingerprints decay rather rapidly within 0.2 ns to yield new transients. The transient, which develops with a time constant of 0.15 ± 0.05 ns in the

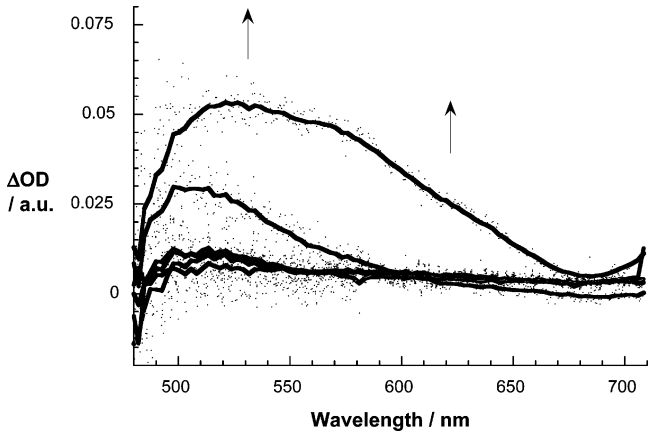

Figure 9. Differential absorption spectrum (visible) obtained upon picosecond flash photolysis (355 nm) of $C_{60}F_{15}$−perylene dyad ($\sim 1.0 \times 10^{-5}$ M) in nitrogen-saturated DCM with several time delays between 50 and 200 ps at room temperature. The spectrum corresponds to the changes that are associated with the transformation of the perylene singlet excited state to the radical ion-pair state.

case of $C_{60}F_{15}$−pyrene, is a close match of the singlet−singlet feature of $C_{60}F_{15}$−*m*-dimethoxybenzene, suggesting a rapid and efficient (i.e., >95%) transduction of singlet excited-state energy. Further evidence for this assignment was lent from nanosecond experiments, where a spectrum evolves that is qualitatively and quantitatively identical with that of the long-lived $C_{60}F_{15}$−*m*-dimethoxybenzene triplet (18 ± 1 μs).

For $C_{60}F_{15}$−perylene, similar decay kinetics, namely, 0.14 ± 0.05 ns, were registered. However, the spectral changes at the conclusion of the perylene singlet decay process are distinctly different from the singlet of $C_{60}F_{15}$−*m*-dimethoxybenzene, which is formed upon photoexcitation of $C_{60}F_{15}$−pyrene. The particularly characteristic transient bleach between 600 and 700 nm is absent. Moreover, the maximum around 535 nm bears close resemblance with the one-electron oxidized radical cation of perylene.[15] This leads us to the hypothesis that electron transfer, rather than energy transfer, governs the fate of the photoexcited perylene moiety in $C_{60}F_{15}$−perylene. Also in this case, the radical ion pair is short-lived with a lifetime of 5.3 ± 0.5 ns (1.9×10^8 s^{-1}), and its decay results in the full recovery of the singlet ground state.

Arguments concerning a possible rationale for the different electron- and energy-transfer behavior should be based on thermodynamic evaluations of the free energy gap changes. From the fluorescence measurements we can evaluate the singlet excited-state energies as the average difference between long-wavelength absorption and short-wavelength fluorescence. In particular, we derive the following values for the photoexcited chromophores: pyrene, 3.3 eV; perylene, 2.6 eV; $C_{60}F_{15}$−*m*-dimethoxybenzene, 1.8 eV. Neglecting electrostatic interactions in the radical ion pairs, we estimate the energy of the charge-separated states by simply adding the first reduction potential of the electron acceptor and the first oxidation potentials of the different electron donors.[15] In doing so we obtain values of 1.51, 0.97, and 0.54 eV for $C_{60}F_{15}$−pyrene, $C_{60}F_{15}$−perylene, and $C_{60}F_{15}$−ferrocene.

With these data in hand the free energy changes for intramolecular electron- and energy-transfer deactivation in $C_{60}F_{15}$−pyrene are extrapolated as 1.79 and 1.5 eV, respectively. For $C_{60}F_{15}$−perylene the corresponding values are 1.63 and 0.8 eV. Evidently, all processes are thermodynamically feasible due to sufficiently large driving forces. In the case of pyrene it is safe to assume that the electron transfer is in the inverted region

SCHEME 2: Energy Diagrams for Trannulene-Based Donor−Acceptor Ensembles (See Text for Exact Energy Levels)

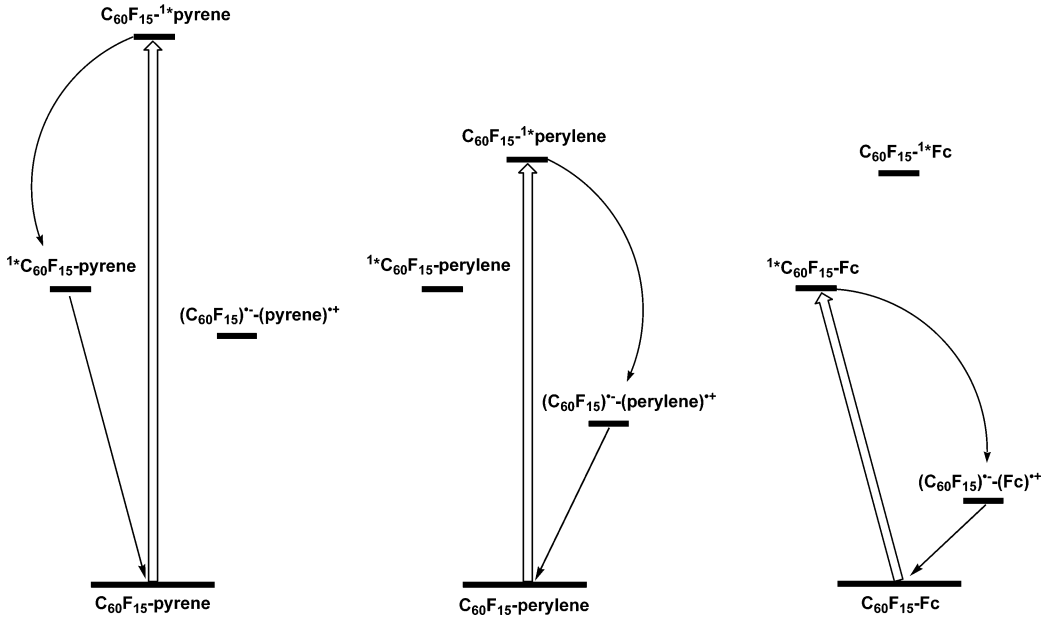

of the Marcus parabola. Thus, electron transfer is not able to compete with the fast and efficient energy transfer across a rather large energy gap. Interestingly, we see no electron transfer evolving from the fullerene singlet excited state. When considering perylene, the thermodynamic considerations are already changed. While the electron transfer—although seemingly still located in the inverted region—is closer to the thermodynamic maximum, the energy gap for energy transfer is markedly decreased. The synergy of these differences leads to a suppression of the energy-transfer deactivation.

More straightforward is the situation for $C_{60}F_{15}$−ferrocene, where the electron-transfer driving force is exothermic (i.e., downhill by ∼1.26 eV),[16] while a transduction of singlet excited-state energy is largely endothermic (i.e., uphill by ∼0.65 eV). Consequently, electron transfer evolves as the only appreciable process. Please note that the only energetically feasible energy-transfer reaction implies formation of the ferrocene triplet (1.35 eV).[17] However, we found no measurable evidence for such an intramolecular energy transfer.[18]

Conclusions

A series of novel trannulene-based donor−acceptor ensembles were tested in a series of steady-state and time-resolved photophysical experiments, complemented by electrochemical studies. Key to the use of trannulenes is their outstanding electron-accepting ability with first reduction potentials at around −0.1 V versus SCE in tetrachloroethane. As electron donors—either in their excited state or in their ground state—pyrene (+1.41 V), perylene (+0.89 V), or ferrocene (+0.44 V) was selected. Depending on the relative energies of the lowest excited state or of the charge-separated state, the outcome of the excited-state chromophore deactivation is either an energy- (i.e., $C_{60}F_{15}$−pyrene) or an electron-transfer (i.e., $C_{60}F_{15}$−perylene and $C_{60}F_{15}$−ferrocene) scenario, which proceed with quantum efficiencies (Φ) of 99.4% ($C_{60}F_{15}$−perylene), 95.3% ($C_{60}F_{15}$−pyrene), and 71.5% ($C_{60}F_{15}$−ferrocene). A summary of the corresponding energy diagrams is given in Scheme 2.

The general photoreactivity, namely, energy-transfer versus electron-transfer products of trannulenes $C_{60}F_{15}Y_3$ (−0.54 V versus Fc/Fc^+) resembles that found for $C_{59}N$ (−1.1 V versus Fc/Fc^+)[15,20,21] and C_{60} derivatives (−1.16 V versus Fc/Fc^+),[22,23] despite their vastly different reduction potentials. Although the fact that the donor−acceptor arrangements (i.e., distance, orientation, and flexibility, etc.) are, in a strict sense, not comparable, an evident trend toward lower quantum efficiencies is discernible for the trannulenes. An obvious reason is found when considering the thermodynamic energy gap dependence of the charge separation, which in the case of the trannulenes (i.e., $-\Delta G \sim 1.26$ eV) is pushed into the inverted region (i.e., $\lambda \sim 0.6-0.7$ eV). This implements a significant activation barrier for initial charge separation, while for $C_{59}N$ and C_{60} derivatives this proceeds essentially activation free.

Experimental Section

Materials. All materials were reagent grade chemicals. Tetrabutylammonium hexafluorophosphate ($(TBA)PF_6$, puriss from Fluka) was used as supporting electrolyte as received. Tetrabutylammonium hexafluoroarseniate ($(TBA)AsF_6$) was synthesized by metathesis reactions from tetrabutylammonium bromide with lithium hexafluoroarseniate (from Aldrich) and twice recrystallized following the procedures reported in the literature.[13] Solvents dichloromethane (DCM, purum, Fluka) and tetrachloroethane (TCE, purum, Fluka) were refluxed over and successively distilled from B_2O_3 and activated 4 Å molecular sieves. They were stored in specially designed Schlenk flasks over 3 Å activated molecular sieves, protected from light, and kept under vacuum prior to use. For the electrochemical experiments, the solvent was distilled into the electrochemical cell, prior to use, using a trap-to-trap procedure.

Electrochemical Instrumentation and Measurements. The one-compartment electrochemical cell was of airtight design, with high-vacuum glass stopcocks fitted with either Teflon or Kalzed (DuPont) O-rings, to prevent contamination by grease. The connections to the high-vacuum line and to the Schlenck containing the solvent were obtained by spherical joints also fitted with Kalzed O-rings. The cell, containing the supporting electrolyte and the electroactive compound, was dried under vacuum at 370 K for at least 48 h. Afterward the solvent was distilled by a trap-to-trap procedure into the electrochemical cell just before performing the electrochemical experiment. The pressure measured in the electrochemical cell prior to performing the trap-to-trap distillation of the solvent was typically (1.0−

2.0) $\times$ 10^{-5} mbar. The working electrode was a Pt disk ultramicroelectrode (diameter, 125 μm) sealed in glass. The counter electrode consisted of a platinum spiral, and the quasi-reference electrode was a silver spiral. The quasi-reference electrode drift was negligible for the time required by a single experiment. Both the counter and the reference electrodes were separated from the working electrode by ~0.5 cm. Potentials were measured with respect to the ferrocene standard. $E_{1/2}$ values correspond to $(E_{pc} + E_{pa})/2$ from CV. Ferrocene was also used as an internal standard for checking the electrochemical reversibility of a redox couple.

Voltammograms were recorded with a custom-made fast potentiostat[19] controlled by an AMEL Model 568 function generator. Data acquisition was performed by a Nicolet Model 3091 digital oscilloscope interfaced to a PC. Temperature control was accomplished within 0.1 K with a Lauda RL6 thermostat.

Spectroelectrochemical measurements were carried out using a quarz OTTLE (optical transparent thin layer electrode) cell with a 0.03 cm path length and a reservoir area attached to the top to hold reference and counter electrodes. Temperature control was achieved by a special cell holder with quartz windows and two nitrogen flows (one at room temperature and the other at low temperature) independently regulated by two needle valves attached to two flow meters (Jencons, item 3015-045). The temperature of the cuvette was monitored with a thermocouple connected to a CAL-9000 digital thermometer and can be tuned between room temperature and 230 K, with an accuracy better than $\pm$0.2 K. The working electrode was a Pt−Rh (90:10) gauze with an optical transparency of about 40%. The counter electrode was a thick Pt wire and a Ar/AgCl electrode, separated by a glass-frit, was the reference one. The potential was set using an AMEL model 552 potentiostat connected to an AMEL model 568 function generator. All the spectra were recorded by a Varian Cary 5, UV−vis−near-IR spectrophotometer. The pristine absorption spectrum was recovered upon reoxidation (at 0 V), showing the reversibility of the reduction process on the time scale of the electrolysis experiment.

Photophysics. Picosecond laser flash photolysis experiments were carried out with 532 nm laser pulses from a mode-locked, Q-switched Quantel YG-501 DP Nd:YAG laser system (pulse width, 18 ps; 2−3 mJ/pulse). Nanosecond laser experiments were performed with laser pulses from a Molectron UV-400 nitrogen laser system (337.1 nm, 8 ns pulse width, 1 mJ/pulse) or from a Qunta-Ray CDR Nd:YAG system (355 nm, 20 ns pulse width). The photomultiplier output was digitized with a Tektronix 7912 AD programmable digitizer. For all photophysical experiments an error of 10% must be considered.

Fluorescence lifetimes were measured with a Laser Strope fluorescence lifetime spectrometer (Photon Technology International) with 337 nm laser pulses from a nitrogen laser fiber coupled to a lens-based T-formal sample compartment equipped with a stroboscopic detector. Details of the Laser Strobe systems are described on the manufacturer's web site, http://www.pti-nj.com.

Emission spectra were recorded with a SLM 8100 spectrofluorometer. The experiments were performed at room temperature. When measuring the fullerene emission in the 700 nm region, a 570 nm long-pass filter in the emission path was used in order to eliminate the interference from the solvent and stray light for recording the fullerene fluorescence. Each spectrum was an average of at least five individual scans, and the appropriate corrections were applied. The fluorescence quantum yields were determined with a 9,10-diphenylanthracene reference (Aldrich, 99+%) (Φ = 1) and an average value of three fluorophore concentrations with optical densities (ODs) at the excitation wavelength ranging from 0.1 to 0.5.

Acknowledgment. This work was carried out with partial support from the EU (RTN network "WONDERFULL"), MIUR (PRIN and FIRB), SFB 583, FCI, EPSRC, the University of Bologna, and the Office of Basic Energy Sciences of the U.S. Department of Energy. This is document NDRL-4628 from the Notre Dame Radiation Laboratory. We wish to dedicate this work to Professor Rudi van Eldik on the occasion of his 60th birthday.

Supporting Information Available: Fluorescence spectra of the $C_{60}F_{15}$−*m*-dimethoxybenzene/$C_{60}F_{15}$−ferrocene, differential absorption spectrum of $C_{60}F_{15}$−*m*-dimethoxybenzene, and differential electronic absorption spectrum of ferrocene. This material is available free of charge via the Internet at http://pubs.acs.org.

References and Notes

(1) (a) Guldi, D. M. *Chem. Soc. Rev.* **2002**, *31*, 22−36. (b) Gust, D.; Moore, T. A.; Moore, A. L. *J. Photochem. Photobiol., B* **2000**, *58*, 63−71. (c) Gust, D.; Moore, T. A.; Moore, A. L *Acc. Chem. Res.* **2001**, *34*, 40−48. (d) Gust, D. Moore, T. A.; Moore, A. L. *Res. Chem. Intermed.* **1997**, *23*, 621−651. (e) Gust, D.; Moore, T. A.; Moore, A. L. *Acc. Chem. Res.* **1993**, *26*, 198−205.

(2) (a) Gust, D.; Moore, T. A. *Top. Curr. Chem.* **1991**, *159*, 103−151. (b) Loewe, R. S.; Tomizaki, K.; Youngblood, W. J.; Bo, Z. S.; Lindsey, J. S. *J. Mater. Chem.* **2002**, *12*, 3438−3451. (c) Tomizaki, K.; Loewe, R. S.; Kirmaier, C.; Schwartz, J. K.; Retsek, J. L.; Bocian, D. F.; Holten, D.; Lindsey, J. S. *Acc. Chem. Res.* **2000**, *33*, 695−703.

(3) (a) Wei, X.-W.; Darwish, A. D.; Boltalina, O. V.; Hitchcock, P. B.; Street, J. M.; Taylor, R. *Angew. Chem., Int. Ed.* **2001**, *40*, 2989−2992. (b) Wei, X.-W.; Avent, A. G.; Boltalina, O. V.; Darwish, A. D.; Fowler, P. W.; Sandall, J. P. B.; Street, J. M.; Taylor, R. *J. Chem. Soc., Perkin Trans. 2* **2002**, 41−46. (c) Darwish, A. D.; Kuvytchko, I. V.; Wei, X.-W.; Boltalina, O. V.; Gold't, I. V.; Street, J. M.; Taylor, R. *J. Chem. Soc., Perkin Trans. 2* **2002**, 1118−1121.

(4) Guldi, D. M.; Prato, M. *Acc. Chem. Res.* **2000**, *33*, 695−703.

(5) (a) Diederich, F.; Kessinger, R. *Acc. Chem. Res.* **1999**, *32*, 537−545. (b) Fullerenes and Related Structures. In *TopIcs in Current Chemistry*, Vol. 199; Hirsch, A., Ed.; Springer, Berlin, 1999. (c) Prato, M.; Maggini, M. *Acc. Chem. Res.* **1998**, *31*, 519−526. (d) *Lecture Notes on Fullerenes Chemistry*; Taylor, R., Ed.; Imperial College Press: London, 1999.

(6) Echegoyen, L.; Echegoyen, L. E. *Acc. Chem. Res.* **1998**, *31*, 593−601.

(7) (a) Zhou, F.; Van Berkel, G. F.; Donovan, B. T. *J. Am. Chem. Soc.* **1994**, *116*, 5485−5486. (b) Liu, N.; Morio, Y.; Okino, F.; Touhara, H.; Boltalina, O. V.; Pavlovich, V. K. *Synth. Metals* **1997**, *86*, 2289−2290. (c) Ohkubo, K.; Taylor, R.; Boltalina, O. V.; Ogo, S.; Fukuzumi, S. *Chem. Commun.* **2002**, 1952−1953. (d) Paolucci, D.; Paolucci, F.; Marcaccio, M.; Carano, M.; Taylor, R. *Chem. Phys. Lett.* **2004**, *400*, 389.

(8) (a) Burley, G. A.; Avent, A. G.; Boltalina, O. V.; Gol'dt, I. V.; Guldi, D. M.; Marcaccio, M.; Paolucci, D.; Paolucci, F.; Taylor, R. *Chem. Commun.* **2003**, 148−149. (b) Burley, G. A.; Avent, A. G.; Boltalina, O. V.; Drewello, T.; Gol'dt, I. V.; Marcaccio, M.; Paolucci, F.; Paolucci, D.; Street, J. M.; Taylor, R. *Org. Biomol. Chem.* **2003**, *1*, 2015−2023. (c) Burley, G. A.; Avent, A. G.; Goldt, I. V.; Hitchcock, P. B.; Al-Matar, H.; Paolucci, D.; Paolucci, F.; Fowler, P. W.; Soncini, A.; Street, J. M.; Taylor, R. *Org. Biomol. Chem.* **2004**, *2*, 319−329.

(9) Burley, G. A.; Fowler, P. W.; Soncini, A.; Sandall, J. P. B.; Taylor, R. *Chem. Commun.* **2003**, 3042−3043.

(10) Bruno, C.; Doubitski, I.; Marcaccio, M.; Paolucci, F.; Paolucci, D.; Zaopo, A. *J. Am. Chem. Soc.* **2003**, *125*, 15738−15739.

(11) Bard, A. J.; Faulkner, L. R. *Electrochemical Methods. Fundamentals and Applications*; Wiley: New York, 2001; Chapter 12 and pp 200−201.

(12) Murrov, S. L.; Carmichael, I.; Hug, G. L. *Handbook of Photochemistry*; Dekker: New York, 1993.

(13) (a) Bard, A. J.; Chlistunoff, J. B. *Inorg. Chem.* **1992**, *31*, 4582−4587. (b) Geiger, W. E.; LeSuer, R. J. *Angew. Chem., Int. Ed.* **2000**, *39*, 248−250.

(14) Steren, C. A.; van Willigen, H.; Biczok, L.; Gupta, N.; Linschitz, H. *J. Phys. Chem.* **1996**, *100*, 8920−8926.

(15) Hauke, F.; Hirsch, A.; Liu, S.-G.; Echegoyen, L.; Swartz, A.; Luo, C.; Guldi, D. M. *Chem. Phys. Chem.* **2002**, *3*, 195−205, and references therein.

(16) The energy of the ferrocene singlet excited state is 2.46 eV—see: Sohn, Y. S.; Hendrickson, D. N.; Gray, H. B. *J. Am. Chem. Soc.* **1971**, *93*, 3603−3609.

(17) (a) Maciejewski, A.; Jaworska-Augustyniak, A.; Szeluga, Z.; Wojtczak, J.; Karolczak, J. *Chem. Phys. Lett.* **1988**, *153*, 227−232. (b) Jaworska-Augustyniak, A.; Karolczak, J.; Maciejewski, A.; Wojtczak, J. *Chem. Phys. Lett.* **1987**, *137*, 134−138. (c) Lee, E. J.; Wrighton, M. S. *J. Am. Chem. Soc.* **1991**, *113*, 8562−8564. (d) Balzani, V.; Bolletta, F.; Scandola, F. *J. Am. Chem. Soc.* **1980**, *102*, 2152−2163.

(18) In line, with a rapid triplet−ground-state deactivation (i.e., triplet lifetime of 0.6 ns), we should not be able to detect any appreciable triplet features at time delays exceeding 1 ns.

(19) Amatore, C.; Jutand, A.; Pfluger, F. *J. Electroanal. Chem.* **1987**, *218*, 361−365.

(20) Hauke, F.; Guldi, D. M.; Hirsch, A. *J. Mater. Chem.* **2002**, *12*, 2088.

(21) (a) Guldi, D. M.; Hauke, F.; Hirsch, A. *Res. Chem. Intermed.* **2002**, *28*, 817. (b) Hauke, F.; Herranz, M. A.; Echegoyen, L.; Guldi, D. M.; Hirsch, A.; Atalick, S. *Chem. Commun.* **2004**, 600. (c) Hauke, F.; Atalick, S.; Guldi, D. M.; Mack, J.; Scott, L.; Hirsch. A. *Chem. Commun.* **2004**, 766. (d) Hauke, F.; Hirsch, A.; Atalick, S.; Guldi, D. M. *Eur. J. Org. Chem.* **2005**, 1741.

(22) (a) Guldi, D. M.; Maggini, M.; Scorrano, G.; Prato, M. *J. Am. Chem. Soc.* **1997**, *119*, 974. (b) Imahori, H.; Tamaki, K.; Guldi, D. M.; Luo, C.; Fujitsuka, M.; Ito, O.; Sakata, Y.; Fukuzumi, S. *J. Am. Chem. Soc.* **2001**, *123*, 2607. (c) Even, M.; Heinrich, B.; Guillon, D.; Guldi, D. M.; Prato, M.; Deschenaux, R. *Chem. Eur. J.* **2001**, *7*, 2595. (d) Bianco, A.; Corvaja, C.; Crisma, M.; Guldi, D. M.; Maggini, M.; Sartori, E.; Toniolo, C. *Chem. Eur. J.* **2002**, *8*, 1544. (e) Guldi, D. M.; Luo, C.; Da Ros, T.; Bosi, S.; Prato, M. *Chem. Commun.* **2002**, 2320. (f) Guldi, D. M.; Luo, C.; Kotov, N. A.; Da Ros, T.; Bosi, S.; Prato, M. *J. Phys. Chem. B* **2003**, *107*, 7293.

(23) (a) Guldi, D. M.; Torres-Garcia, G.; Mattay, J. *J. Phys. Chem. A* **1998**, *102*, 9679. (b) Kordatos, K.; Da Ros, T.; Prato, M.; Luo, C.; Guldi D. M. *Chem. Mon.* **2001**, *132*, 63.